Nuclear Science and Techniques (2026) 37:34
https://doi.org/10.1007/s41365-025-01851-9

Investigation of the production of ^{152}Tb and ^{155}Tb terbium radioisotopes with europium targets

C. Yalçın[1]

Received: 27 July 2024 / Revised: 27 December 2024 / Accepted: 13 March 2025 / Published online: 5 January 2026

Abstract
In recent years, terbium radioisotopes have been investigated for their potential therapeutic and diagnostic applications in nuclear medicine. This study aimed to investigate the production of ^{152}Tb and ^{155}Tb by alpha-induced reactions in detail, with a specific focus on determining the optimum production parameters and testing existing nuclear models. Given the limited number of experiments conducted on reactions related to terbium isotope production, it is necessary to perform theoretical calculations of cross sections over a wide energy range to gain a detailed understanding of terbium isotope production. To achieve this objective, the cross sections of the ^{151}Eu(α,n)^{154}Tb reactions were calculated up to 60 MeV using the TALYS computer code with 432 different combinations of optical model parameters, level density, and strength function models. The theoretical reaction cross-section results were compared with the experimental results in the literature. The best input parameters were determined using the Threshold Logic Unit method, and these parameters were used in all isotope production calculations. Once the optimal model combination was determined, the total activity production and isotopic fraction of ^{152}Tb and ^{155}Tb isotopes were calculated in detail for beam energies of 17–50 MeV, different irradiation times, and varying ^{151}Eu and ^{153}Eu target thicknesses.

Keywords Terbium radioisotopes · Medical isotope production · Alpha-induced reactions · Cross section · Threshold logic unit method

1 Introduction

A multitude of medical radioisotopes, including ^{18}F, ^{99m}Tc, ^{68}Ga, and ^{177}Lu, are currently used for diagnostic and therapeutic purposes. However, in recent years, novel radioisotopes have been proposed that exhibit numerous advantages over existing radioisotopes. In particular, the utilization of radiolanthanides in nuclear medicine has been the subject of numerous in vitro and in vivo studies [1]. In a recent preclinical study, Müller et al. [2] investigated the combined use of ^{149}Tb, ^{152}Tb, ^{155}Tb, and ^{161}Tb radioisotopes. These radionuclides are distinctive in that they exhibit properties suitable for positron emission tomography (PET), single−photon emission computed tomography (SPECT), and radionuclide therapy, the three principal modalities of nuclear medicine. Müller et al. employed a folate-based targeting agent comprising a dodecane tetraacetic acid (DOTA) chelator to facilitate the binding of Tb to the biomolecule, and reported highly promising results [2]. Imaging of folate receptor (FR) positive human tumors xenografted into mice with both ^{152}Tb (PET, 17% β^+) and ^{155}Tb (SPECT) has been demonstrated to be of high quality. Furthermore, the same compound, labeled with therapeutic ^{149}Tb and ^{161}Tb, demonstrated the potential to cure the disease.

The primary production method for ^{161}Tb is the irradiation of ^{160}Gd with thermal neutrons in a reactor [3]. The production of ^{149}Tb, ^{152}Tb, and ^{155}Tb may be accomplished using charged-particle accelerators. An overview of ^{149}Tb production methods can be found in [4–7], whereas an overview of ^{155}Tb production methods can be found in [8]. The production of ^{152}Tb can be achieved through the irradiation of Gd and Eu isotopes with protons [9–11], deuterons [12] and alphas [13, 14], as well as spallation reactions initiated by high-energy protons [15].

✉ C. Yalçın
caner.yalcin@kocaeli.edu.tr

[1] Department of Physics, Kocaeli University, Umuttepe, 41001 Kocaeli, Turkey

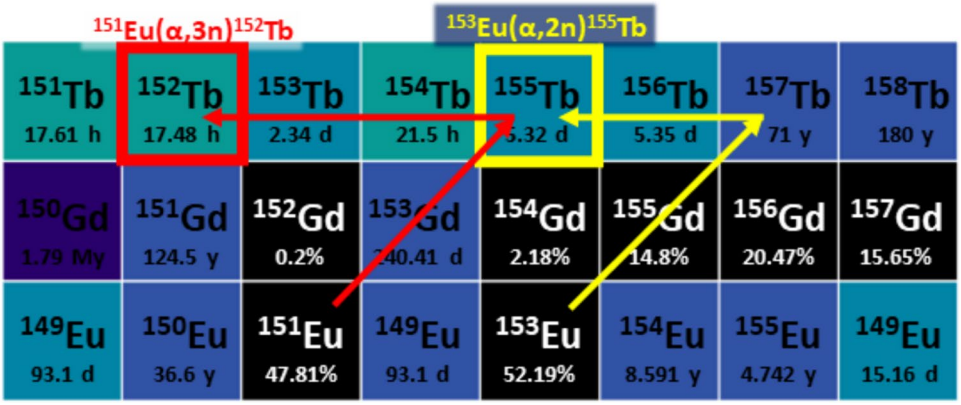

Fig. 1 (Color online) The relevant part of the isotope table and the production route to be used for the production of the medical isotopes ^{152}Tb and ^{155}Tb

Table 1 Optical model potentials (OMP), which are available in the Talys code. The default options for OMP is the Avrigeanu et al. (2014) (OMP-6)[31]

Model no	Optical model potential
OMP-1	Normal alpha potential (1958) [28]
OMP-2	McFadden and Satchler (1966) [29]
OMP-3	Demetriou et al. (2002) (table 1) [30]
OMP-4	Demetriou et al. (2002) (table 2) [30]
OMP-5	Demetriou et al. (2002) (dispersive model) [30]
OMP-6	Avrigeanu et al. (2014) [31]
OMP-7	Nolte et al. (1987) [32]
OMP-8	Avrigeanu et al. (1994) [33]

Table 2 Level density models(LDM) which are available in the Talys code. The default options for LDM is constant temperature + Fermi gas model (LDM-1) [34]

Model no	Level density model
LDM-1	Constant temperature + Fermi gas model [34]
LDM-2	Back-shifted Fermi gas model [35, 36]
LDM-3	Generalized superfluid model [37, 38]
LDM-4	Microscopic level densities (Skyrme force) [39] from Goriely's tables
LDM-5	Microscopic level densities (Skyrme force) [40] from Hilaire's combinatorial tables
LDM-6	Microscopic LD (temp. dependent HFB, Gogny force) from Hilaire's combinatorial tables (2014) [41]

Table 3 Gamma-ray strength function models (SFM) which are available in the Talys code. The default options for SFM is the Brink-Axel Lorentzian model (SFM-2) [44, 45]

Model no	Strength function model
SFM-1	Kopecky-Uhl generalized Lorentzian [42, 43]
SFM-2	Brink-Axel Lorentzian [44, 45]
SFM-3	Hartree-Fock BCS tables [46]
SFM-4	Hartree-Fock-Bogolyubov tables [47]
SFM-5	Goriely's hybrid model [48]
SFM-6	Goriely T-dependent HFB [51]
SFM-7	T-dependent RMF [49]
SFM-8	Gogny D1M HFB+QRPA [50]
SFM-9	Simplified Modified Lorentzian (SMLO) [52]

Although several experimental studies have been conducted on the production of medical Tb isotopes, an appropriate production mechanism has not yet been fully proposed. In cases where experimental studies are insufficient, the combination of theoretical investigations with experiments can be a helpful approach. To study isotope production theoretically, the reaction cross sections in the region of interest must be well known. Theoretical cross sections can be calculated using the Hauser-Feshbach statistical model. In these calculations, parameters such as the optical model, level densities, and strength function were employed. As these parameters have not yet been determined globally, they vary according to the mass and energy regions of interest. All of these models affect the theoretical cross-section calculations, particularly in the low-energy region, where the optical α-nucleus potential is likely to introduce the most significant deviations in the charged-particle reactions [16–19]. The parameters proposed thus far are listed in Tables 1, 2, and 3. Consequently, it is essential to determine which models should be used for theoretical cross-section calculations. To ascertain which models are most appropriate for use in the region of interest, the ^{151}Eu(α,n)^{154}Tb reaction cross section was subjected to a detailed analysis and compared with the experimental results of Gyürky et al. [13], which exhibited the lowest energy and cross-section uncertainties. A total of 432 different combinations of eight optical potentials, six level densities, and nine strength function models were subjected to reaction cross-section calculations, which were then compared with experimental results. The Threshold Logic Unit method [16, 20] was used to determine the best model parameters.

In the present study, the cross sections of the alpha-induced reactions of ^{151}Eu(α,3n)^{152}Tb and ^{151}Eu(α,2n)^{153}Tb and ^{151}Eu(α,n)^{154}Tb and ^{153}Eu(α,2n)^{155}Tb were calculated with best model parameters for the production of ^{152}Tb and ^{155}Tb. Optimal production parameters for ^{152}Tb and ^{155}Tb have been proposed for commercial cyclotron accelerators. This work can be studied not only in medical physics but also in other fields where knowledge of reaction cross sections is required, such as nuclear astrophysics [16, 21–25] and nuclear technology [26].

2 Method and calculation

2.1 Cross-section calculations

The cross sections for the ^{151}Eu(α,n)^{154}Tb reaction were predicted using the TALYS 1.96 computer code [27], which employs Hauser-Feshbach statistical model calculations. Optical model potentials (OMP), level density models (LDM), and strength function models (SFM) play significant roles in theoretical cross-section calculations. For further details regarding the models, please refer to the relevant literature. To investigate the sensitivities of these parameters to the reaction cross sections, calculations were performed for combinations of eight OMP, six LDM, and nine SFMs, as presented in Tables 1, 2, and 3 [28–52]. Once the optimal model was identified, the reaction pathways illustrated in Fig. 1 and the synthesis of ^{152}Tb and ^{155}Tb were subjected to further analysis [53].

OMPs is a major input parameter for calculating the cross section. The OMPs used in the calculations, labeled with OMP-1 through OMP-8, are normal alpha potential [28], McFadden and Satchler [29], Demetriou et al. [30], Avrigeanu et al. [31] which is the default option of the code, Nolte et al. [32], Avrigeanu et al. [33].

Three microscopic and three phenomenological level density models were included in the calculations. The phenomenological LDMs are constant temperature + Fermi gas model [34], back-shifted Fermi gas model [35, 36] and generalized superfluid model [37, 38], labeled with LDM-1 through LDM-3. Two microscopic LDMs were chosen using the Skyrme force from Goriely's (LDM-4) [39] and Hilaire's (LDM-5) [40] tables. The third microscopic LDM used the Gogny force from Hilaire's combinatorial tables (LDM-6) [41]. The default option of the code is the Constant Temperature-Fermi Gas Model (LDM-1) [34].

Nine different SFMs were selected for the calculations, labeled SFM-1 through SFM-9, as listed in Table 3. The default option of the SFM is the Brink-Axel Lorentzian model (SFM-2) [44, 45].

2.2 Threshold logic unit method

To identify the most compatible input parameter sets, the threshold logic unit (TLU) method was employed to evaluate 432 combinations of eight OMP, six LDM, and nine SFMs for the alpha-induced reaction of the ^{151}Eu isotope. The TLU method is based on the concept of a binary threshold function. In this approach, each input is multiplied by a weight, and the sum of these weighted inputs is compared with a threshold value, as expressed in Eq. (2) and referenced in [20]. If the sum exceeds the threshold, the TLU outputs 1; otherwise, it outputs 0.

In this study, the input values (X_i) are determined by comparing the TALYS results with the experimental values within twice their uncertainties, as

$$X_i = \begin{cases} 1 & \text{if } \sigma_{\mathrm{E}i} - 2\Delta\sigma_{\mathrm{E}i} \le \sigma_{\mathrm{T}i} \le \sigma_{\mathrm{E}i} + 2\Delta\sigma_{\mathrm{E}i} \\ 0 & \text{otherwise} \end{cases} \quad (1)$$

where $\sigma_{\mathrm{E}i}$ and $\sigma_{\mathrm{T}i}$ are the experimental and TALYS results, respectively, and $\Delta\sigma_{\mathrm{E}i}$ is the experimental uncertainty at energy i.

The obtained binary input values were compared with the threshold τ and the best model combinations BMC were determined, as

$$BMC = \begin{cases} 1 & \text{if } \sum_{i=1}^{n}(\theta_i X_i) \ge \tau \\ 0 & \text{otherwise} \end{cases} \quad (2)$$

where the weight factors (θ_i) are taken as one because the weights of the cross sections are equal at all energies, n is the number of energies at which the experiments were carried out, and the threshold τ is selected as the number of experimental energies at which the TALYS results were accepted with the experimental values within twice their uncertainties, that is, X_i is one, otherwise X_i is zero. The cross sections of the ^{151}Eu(α,n)^{154}Tb reaction were measured at 13 different energies, indicating that n is equal to thirteen. The TLU method was then applied for three threshold values, namely, $\tau = 11$, 12, and 13. The calculation of medical isotope production was performed using the TALYS results, with the objective of identifying the optimal combination of models that were in accordance with the experimental values at all 12 energies. This process revealed that the threshold was 12.

2.3 Production of terbium radioisotopes

Once the most suitable model was selected, the reaction pathways depicted in Fig. 1, along with the production of

^{152}Tb and ^{155}Tb, were calculated using the TALYS code (the reaction data are summarized in Table 4). The total number of the produced nuclei $Y(t)$ during an irradiation time t (t=0 at the beginning of irradiation) is given by following equation [54]

$$\begin{aligned} Y(t) &= t\int_0^L \mathrm{d}x I(x)\sigma(x)\left(\frac{\rho}{Ze}\right) \\ &\cong tI_0\int_{E_{\mathrm{back}}}^{E_{\mathrm{beam}}} \mathrm{d}E\left(-\frac{1}{\rho}\frac{\mathrm{d}E}{\mathrm{d}x}\right)^{-1}\frac{\sigma(E)}{Ze} \\ &\equiv tI_0 y, \end{aligned} \tag{3}$$

where ρ is the target isotope number density, L is the target thickness, I_0 is the number of beam particles irradiating the sample per unit irradiation time, Z is the charge number, and e is the electron charge. E_{beam} denotes the incident beam energy, and E_{back} is the average projectile energy available at the backside of the target. The cross section to produce the isotope at depth x in the sample is $\sigma(x)$, and $-(1/\rho)(\mathrm{d}E/\mathrm{d}x)$ is the stopping power. The y term is the number of produced nuclei following the deposition of the unit induced electric charge.

If the projectiles travel through the target, the average projectile beam energy decreases. The amount of energy loss inside the target is determined by the target thickness and stopping power. The Talys code calculates the stopping power using the Bethe-Bloch formula [55]. The integration limits E_{beam} and E_{back} are fixed by the requested projectile energy range inside the target, which is determined by the cross section as a function of the projectile energy. The spreading of the beam inside the target was neglected. The stopping power describes the average energy loss of projectiles in the target by atomic collisions as a function of their energy in (MeV/cm).

Table 4 The production route and properties of the isotopes under investigation [53]

Isotope	$T_{1/2}$	Reaction	Q-value (MeV)	Decay mode
^{150}Tb	3.48 h	^{151}Eu(α,5n)^{150}Tb	−41.48	$\epsilon+\beta^+$ (100%)
^{151}Tb	17.61 h	^{151}Eu(α,4n)^{151}Tb	−32.89	$\epsilon+\beta^+$ (99.9905%)
				α (0.0095%)
^{152}Tb	16.48 h	^{151}Eu(α,3n)^{152}Tb	−25.72	$\epsilon+\beta^+$ (100%)
^{153}Tb	2.34 d	^{151}Eu(α,2n)^{153}Tb	−17.06	$\epsilon+\beta^+$ (100%)
^{154g}Tb	21.5 h	^{151}Eu(α,n)^{154g}Tb	−10.14	$\epsilon+\beta^+$ (100%)
^{154m1}Tb	9.99 h	^{151}Eu(α,n)^{154m1}Tb	−10.26	$\epsilon+\beta^+$ (78.2%)
				IT (21.8%)
^{154m2}Tb	22.7 h	^{151}Eu(α,n)^{154m2}Tb	−10.54	$\epsilon+\beta^+$ (98.2%)
				IT (1.8%)
^{154g}Tb	21.5 h	^{153}Eu(α,3n)^{154g}Tb	−25.00	$\epsilon+\beta^+$ (100%)
^{154m1}Tb	9.99 h	^{153}Eu(α,3n)^{154m1}Tb	−25.11	$\epsilon+\beta^+$ (100%)
				IT (21.8%)
^{154m2}Tb	22.7 h	^{153}Eu(α,3n)^{154m2}Tb	−25.40	$\epsilon+\beta^+$ (100%)
				IT (1.8%)
^{155}Tb	5.32 d	^{153}Eu(α,2n)^{155}Tb	−15.97	ϵ (100%)
^{156}Tb	5.35 d	^{153}Eu(α,n)^{156}Tb	−9.31	$\epsilon+\beta^+$ (100%)

3 Results and discussion

To study the production of terbium isotopes, it is essential to have a comprehensive understanding of the relevant experimental and theoretical cross sections within the designated energy range. It is regrettable that not all cross sections necessary for the production of terbium isotopes have been experimentally measured at the relevant energies. Consequently, theoretical cross sections may prove to be an efficacious instrument for investigating of radioisotope production. Nevertheless, the accuracy of the calculated theoretical cross sections is not guaranteed, particularly in the case of alpha-initiated reactions. A multitude of parameters are employed to calculate the cross sections. Therefore, it is essential to examine each parameter individually for each nucleus in energy range. In order to ascertain which models are most appropriate for use in the region of interest, the ^{151}Eu(α,n)^{154}Tb reaction cross section was subjected to a detailed analysis and compared with the experimental results of Gyürky et al. [13], which exhibit the lowest energy and cross-section uncertainties. A total of 432 different combinations of eight optical potentials, six level densities, and nine power function models were subjected to reaction cross-section calculations, which were then compared with experimental results. Threshold Logic Unit method [16, 20] was used to determine the best model parameters.

The theoretical results of the ^{151}Eu(α,n)^{154}Tb reaction cross section were calculated with 432 combinations of eight OMP, six LDM, and nine SFM were compared with experimental values [13] measured at thirteen energies. Model Parameters are labeled with $MP-ijk$, where i, j and k represent $OMP-i$, $LDM-j$ and $SFM-k$, respectively, in Tables 1, 2, and 3. In the study employing the TLU method, the optimal combinations (MP-238) were identified, which were in alignment with the experimental results at twelve energies of the thirteen, as illustrated in Fig. 2. The calculated cross-section values are in agreement with the experiment at all points except at 11.99 MeV. The calculated and experimental cross-section values are listed in Table 5.

Furthermore, the model was tested for medical isotope production reactions, specifically the ^{151}Eu(α,2n)^{153}Tb and ^{151}Eu(α,3n)^{152}Tb reactions. As illustrated in Figs. 3 and 4, the outcomes produced by the MP-238 model are in agreement with the experimental findings reported by Moiseeva et al. [14]. Unfortunately, there are no experimental measurements

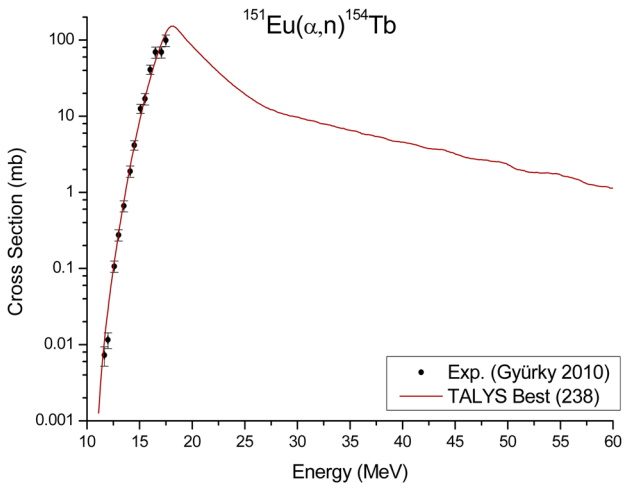

Fig. 2 (Color online) The ^{151}Eu(α,n)^{154}Tb cross sections obtained by TALYS using the best combination (MP-238) selected. The first digit in the legend represents the Optical Model number, the second digit the Level Density model number and the third digit the Strength Function model number (Tables 1, 2, and 3)

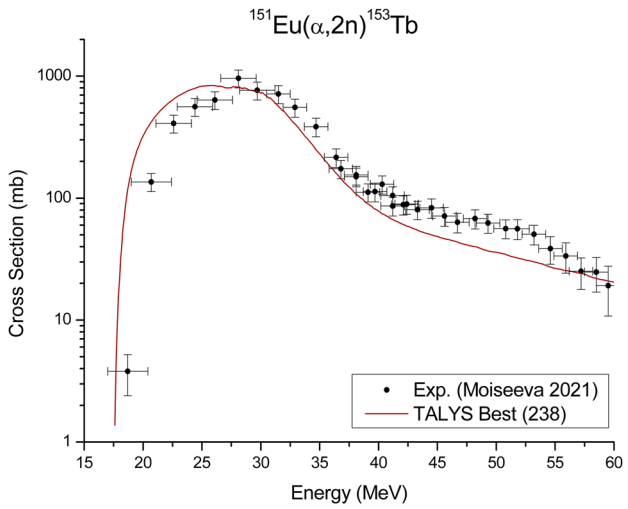

Fig. 3 (Color online) The ^{151}Eu(α,2n)^{153}Tb cross sections obtained by TALYS using the best combination. The explanations same as in Fig. 2

Table 5 Cross sections calculated with MP-238, and experimental values, for ^{151}Eu(α,n)^{154}Tb reaction

$E_{\text{Lab.}}$ (MeV)	TALYS (MP-238) (mb)	Experiment [13] (mb)
11.65 ± 0.04	0.011	0.007 ± 0.002
11.99 ± 0.04	0.029	0.012 ± 0.003
12.59 ± 0.04	0.120	0.11 ± 0.02
13.00 ± 0.04	0.287	0.276 ± 0.047
13.50 ± 0.04	0.758	0.666 ± 0.111
14.10 ± 0.04	2.173	1.898 ± 0.322
14.50 ± 0.04	4.134	4.169 ± 0.580
15.09 ± 0.04	9.829	12.583 ± 1.733
15.51 ± 0.05	17.193	16.932 ± 2.904
16.00 ± 0.05	31.056	41.008 ± 5.759
16.50 ± 0.05	52.976	69.274 ± 11.793
17.07 ± 0.05	89.319	69.490 ± 11.750
17.50 ± 0.05	124.821	99.486 ± 17.256

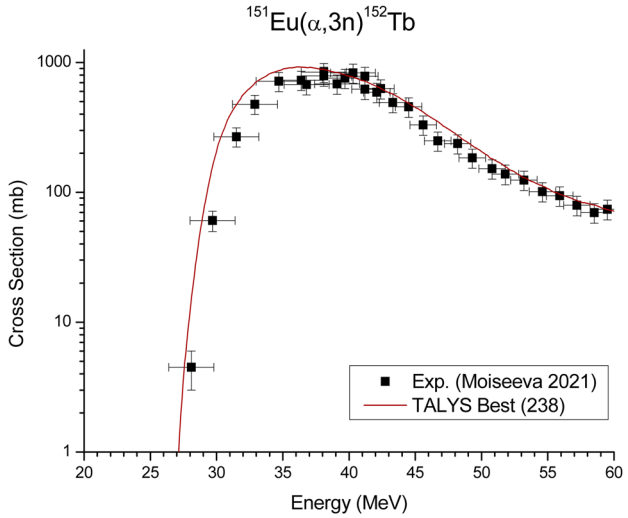

Fig. 4 (Color online) The ^{151}Eu(α,3n)^{152}Tb cross sections obtained by TALYS using the best combination. The explanations same as in Fig. 2

in the literature for the ^{153}Eu(α,2n)^{155}Tb reaction, which is used for ^{155}Tb production. Consequently, the theoretical cross sections could not be compared with the experimental results. For these reactions, MP-238 was assumed to be compatible because of the close mass and properties of the target isotopes of Eu, and this model combination was used in all isotope production calculations.

3.1 The production of ^{152}Tb with ^{151}Eu target

For the production calculation of ^{152}Tb, it was assumed that the enriched ^{151}Eu target was irradiated with an alpha beam in 1 MeV steps starting at 30 MeV up to 50 MeV, and the activities and isotopic fractions of the isotopes produced in all reaction channels were calculated. A comprehensive analysis was conducted to ascertain the impact of irradiation time on the calculated values, spanning from one to 24 h. Additionally, the influence of varying target thicknesses

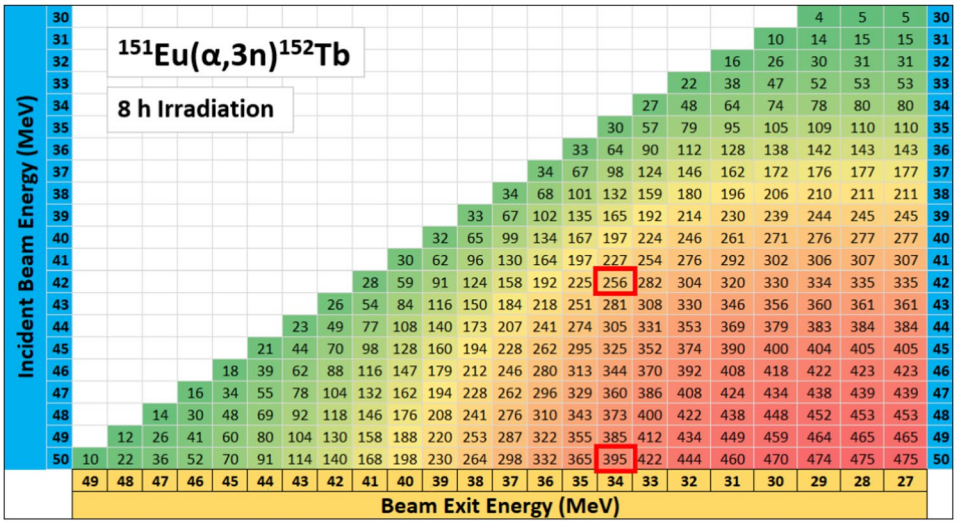

Fig. 5 (Color online) The activity of ^{152}Tb (in MBq/μA) is presented as a function of beam energy and target thickness at a beam current of 1 μA and an irradiation time of 8 h with an enriched ^{151}Eu target. The target thickness was expressed in terms of beam exit energy, and the beam profile was assumed to be 1 cm^2

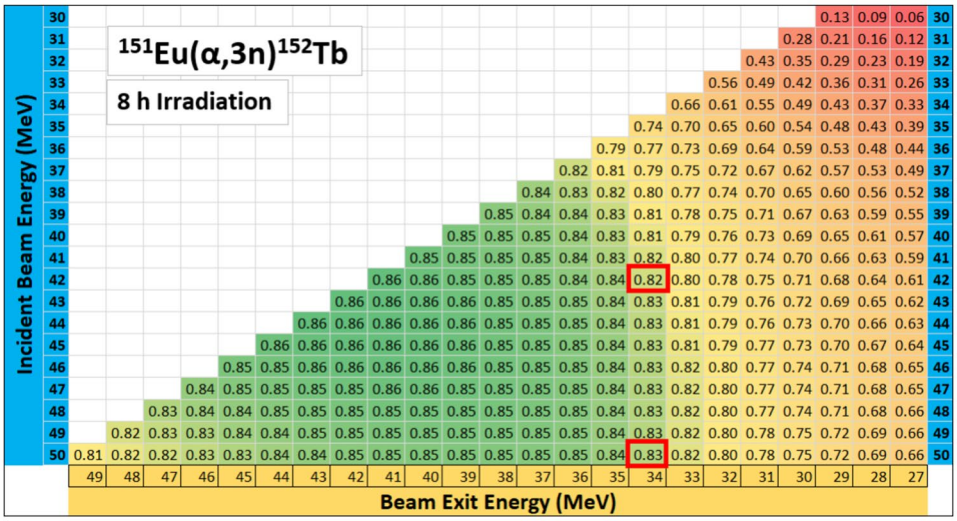

Fig. 6 (Color online) The isotopic fraction of ^{152}Tb with respect to beam energy and target thickness was determined following irradiation with an enriched ^{151}Eu target at a beam current of 1 μA for 8 h. The target thickness is expressed in terms of the beam energy that leaves the target. The beam profile was assumed to be 1 cm^2

on the results was investigated, providing insights into the effects of these variables on the observed outcomes. The results obtained after 8 h of irradiation are shown in Figs. 5 and 6. As Europium is typically present in its oxide form and is known to undergo rapid oxidation, this study assumes that the Eu target is in its oxide form throughout the calculations.

As shown in Fig. 6, with a beam energy of 50 MeV and a target thickness corresponding to an output energy of 34 MeV (corresponding to a 0.26 mm thick target), ^{152}Tb with an isotopic fraction of 0.83 can be produced in 8 h with an activity of 395 MBq/μA (Fig. 5). As the exit energy decreases below 34 MeV, a notable decline in the isotopic fraction and radionuclide purity is observed (Fig. 6). As the irradiation time was extended, the ^{152}Tb fraction was calculated to decrease by approximately 1% every eight hours.

Moiseeva et al. [14] proposed the production of ^{152}Tb with a 42 MeV beam current and 34 MeV beam exit energy. However, as illustrated in Figs. 5 and 6, both the isotopic fraction and activity increase in ^{152}Tb production with 50 MeV beam energy and 34 MeV exit energy. While the isotopic fraction shows only a modest increase, the activity level rises significantly from 256 to 395 MBq/μA. Furthermore, our calculations based on the combination proposed by Moiseeva et al. [14] are in accordance with the experimental findings. The activity reported by Moiseeva et al. [14], 222 MBq/μA, was calculated to be 256 MBq/μA. Figure 7 illustrates the variation in isotopic fractions as a function of target thickness when irradiated with 50 MeV (solid line) and 42 MeV (dashed line) beams. As evidenced by the region highlighted in yellow in the graph, the isotopic fraction exhibited minimal change for ^{152}Tb up to an exit

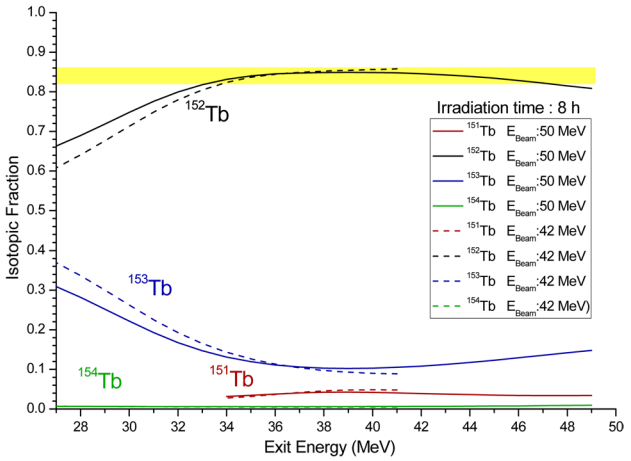

Fig. 7 (Color online) 1 μA beam current and 8 h of irradiation with 42 MeV (dashed line) and 50 MeV (solid line) beam energy and ^{152}Tb isotopic fraction with respect to target thickness. Target thickness is given in terms of beam exit energy

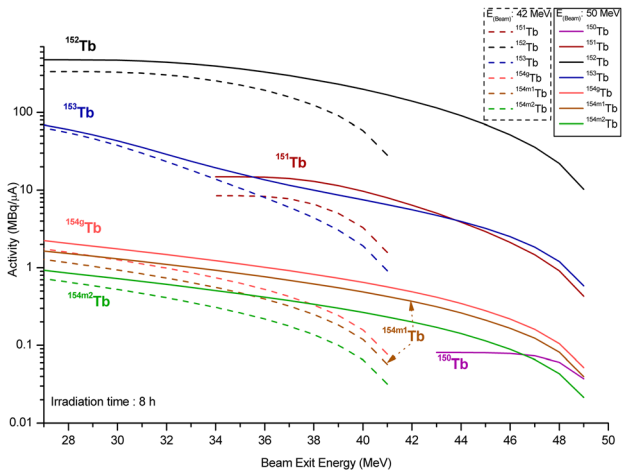

Fig. 8 (Color online) 1 μA beam current and 8 h of irradiation with 42 MeV (dashed line) and 50 MeV (solid line) beam energy and ^{152}Tb activity with respect to target thickness. Target thickness is given in terms of beam exit energy

energy of 34 MeV. Figure 8 illustrates the impact of varying target thicknesses on the produced activity when irradiated with 50 and 42 MeV beams. The threshold energy for the ^{151}Eu(α,4n)^{151}Tb reaction is 33.76 MeV. Therefore, the production of ^{151}Tb is not possible at energies below this threshold. Similarly, ^{150}Tb, which results from the ^{151}Eu(α,5n)^{150}Tb reaction, cannot be produced below the threshold energy of 42.6 MeV. Therefore, Fig. 8 presents only the activity produced by irradiation with a 50 MeV energy beam. The maximum activity obtained for ^{150}Tb is 0.8 MBq/μA.

3.2 The production of ^{155}Tb with ^{153}Eu target

Upon analyzing the production of ^{155}Tb by the reaction ^{153}Eu(α,2n)^{155}Tb, it was observed that the isotopic fraction of ^{155}Tb gradually decreased as the beam energy increased. As illustrated in Fig. 9, the irradiation of the enriched ^{153}Eu target for eight hours with a beam energy of 31 MeV and a beam exit energy of 17 MeV results in the production of ^{155}Tb with a 90% isotopic fraction. Under these conditions, a 37.3 MBq activity will be obtained with a 1 μA beam current. The reaction cross sections for the dominant products formed as a consequence of irradiation with the enriched ^{153}Eu target are shown in Fig. 10.

This process allows the production of both ^{152}Tb and ^{155}Tb isotopes simultaneously. By employing a target design analogous to that depicted in Fig. 11, it is possible to generate ^{152}Tb at high energies and ^{155}Tb at low energies, respectively. The utilization of an Al energy degrader is an effective method for minimizing contamination from other isotopes in the intermediate region, thereby reducing both the irradiation time and production costs. The required thickness of the Al energy degrader for decreasing the beam energy from 34 to 31 MeV was determined using the ThiMeT code [56]. Figure 12 illustrates the activities resulting from 8 h of irradiation and 24 h of decay, as represented by the proposed target design.

4 Conclusion

A computer code using the statistical Hauser-Feshbach approach was used to determine the most compatible theoretical results with the experimental data. The reaction cross sections were calculated using the TALYS code for a total of 432 different combinations of eight optical potentials, six level densities, and nine strength function models. The calculations closest to the experimental results were those obtained with the combinations of MP-238, which was determined using the TLU method. That is, the optical model potential of McFadden and Satchler [29], Generalized superfluid energy level density model by Ignatyuk et al. [37, 38] and the strenght function model of Gogny D1M HFB+QRPA by Martini et al. [50]. The ^{153}Eu(α,2n)^{155}Tb reaction, for which no experimental cross-section data are available in the literature, was the subject of an in-depth study. The predicted cross-section values allowed us to calculate ^{155}Tb production for the first time.

The TLU method can identify the most optimal parameter model for predicting reaction cross sections that align with experimental data. Recently, a considerable number of studies have employed the chi-square test in this field [57].

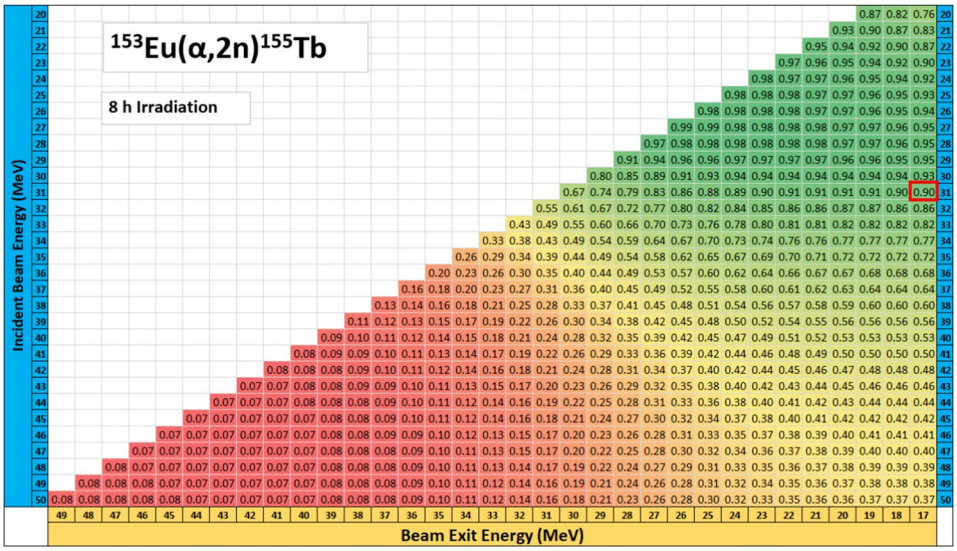

Fig. 9 (Color online) The isotopic fraction of ^{155}Tb with respect to beam energy and target thickness was determined following irradiation with an enriched ^{153}Eu target at a beam current of 1 μA for 8 h. The target thickness is expressed in terms of the beam energy leaving the target. The beam profile was assumed to be 1 cm^2

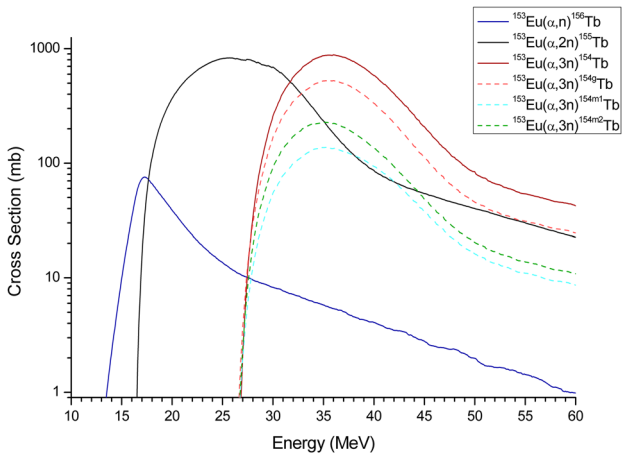

Fig. 10 (Color online) Calculated reaction cross section for the ^{153}Eu target. The dashed lines show the cross section of the ground and two metastable states for reaction ^{153}Eu(α,3n)^{154g,m1,m2}Tb

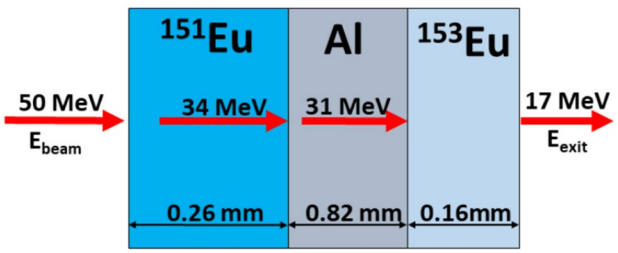

Fig. 11 (Color online) Target design to produce both ^{152}Tb and ^{155}Tb at the same time

The TLU method represents a distinct and straightforward approach that can be utilized in future studies.

To theoretically determine the medical isotope production parameters, it is necessary to have a good understanding of the cross section, stopping power, and decay parameters. The cross sections derived in this study were adequately corroborated by empirical data, and the parameters governing the observed decay were well documented. Currently, no experimental data are available regarding the stopping power of alpha particles in Eu. Consequently, theoretical calculations must be used as the basis for determining these parameters.

Using ^{151}Eu target with a 50 MeV beam energy and 34 MeV exit energy, ^{152}Tb with 83% isotopic fraction and 395 MBq/μA activity can be produced. Similarly, ^{155}Tb with 90% isotopic fraction and 37.3 MBq/μA activity can be produced using ^{153}Eu target with 31 MeV beam energy and 17 MeV exit energy. A target design analogous to that depicted in Fig. 11 was employed to produce ^{152}Tb with an activity of 395 MBq/μA and 37.3 MBq/μA of ^{155}Tb, respectively, utilizing a beam energy of 50 MeV. It should be noted that the aforementioned calculations were conducted with a beam current of 1 μA, and thus, the calculated activities will

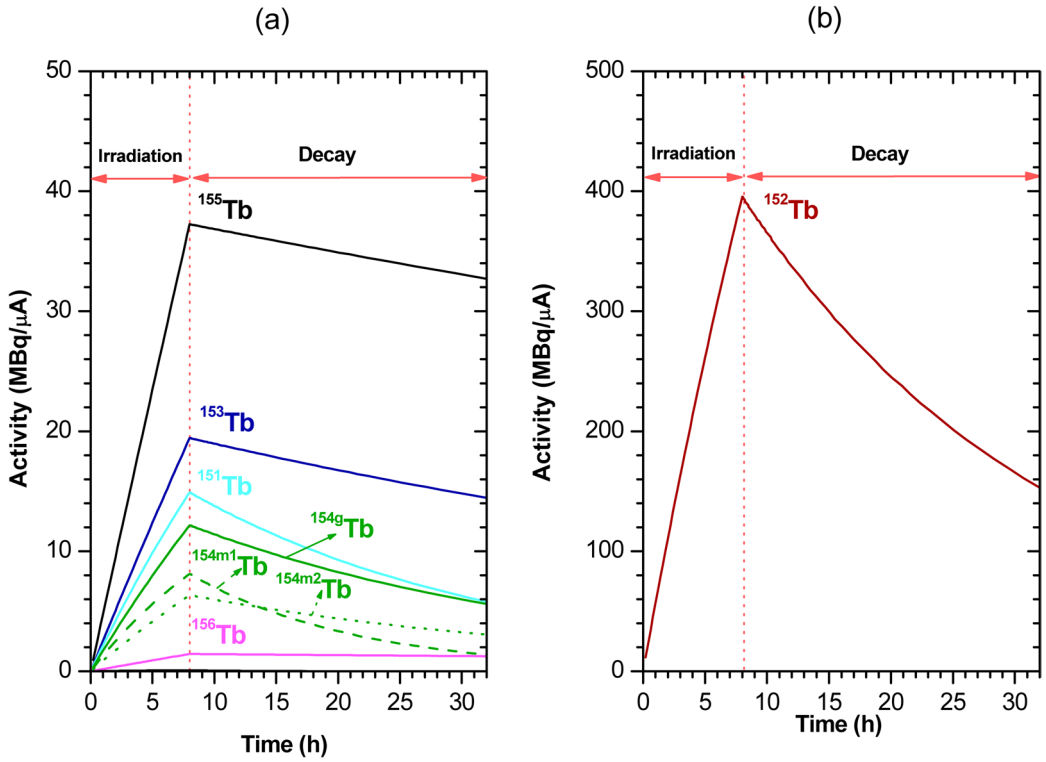

Fig. 12 (Color online) The activity of isotopes formed as a result of 1 μA beam current and 8 h of irradiation using the target design in Fig. 11 and decayed 24 h after irradiation. **a** For the ^{151}Tb, ^{153}Tb, ^{154g,m1,m2}Tb, ^{155}Tb, and ^{156}Tb **b** for the ^{152}Tb

increase in direct proportion to the increase in beam current. The ratio of ^{152}Tb to ^{155}Tb can be modified by allowing the decay of ^{152}Tb.

Further investigations with greater diversity and complexity can be conducted using the proposed model. However, more precise measurements of the experimental cross sections over a broader energy range would enhance theoretical investigations. Therefore, it is imperative to employ the thin target activation method in order to obtain precise cross-section measurements, which are crucial for the analysis of the reactions of interest.

Declarations

Conflict of interest The authors declare that they have no conflict of interest.

References

1. N. Naskar, S. Lahiri, Theranostic terbium radioisotopes: challenges in production for clinical application. Front. Med. **8**, 675014 (2021). https://doi.org/10.3389/fmed.2021.675014
2. C. Müller, A. Singh, C.A. Umbricht et al., Preclinical investigations and first-in-human application of ^{152}Tb-PSMA-617 for PET/CT imaging of prostate cancer. EJNMMI Res. **9**, 68 (2019). https://doi.org/10.1186/s13550-019-0538-1
3. S. Lehenberger, C. Barkhausen, S. Cohrs et al., The low-energy β^- and electron emitter ^{161}Tb as an alternative to ^{177}Lu for targeted radionuclide therapy. Nucl. Med. Biol. **38**, 917–924 (2011). https://doi.org/10.1016/j.nucmedbio.2011.02.007
4. M. Maiti, New measurement of cross sections of evaporation residues from the ^{nat}Pr+^{12}C reaction: A comparative study on the production of ^{149}Tb. Phys. Rev. C **84**, 044615 (2011). https://doi.org/10.1103/physrevc.84.044615
5. S.M. Qaim, B. Scholten, B. Neumaier, New developments in the production of theranostic pairs of radionuclides. J. Radioanal. Nucl. Chem. **318**, 1493–1509 (2018). https://doi.org/10.1007/s10967-018-6238-x
6. G.J. Beyer, J.J. Comor, M. Dakovic et al., Production routes of the alpha emitting ^{149}Tb for medical application. Radiochim. Acta **90**, 247–252 (2002). https://doi.org/10.1524/ract.2002.90.5_2002.247
7. A.N. Moiseeva, R.A. Aliev, V.N. Unezhev et al., Cross section measurements of ^{151}Eu(^{3}He,5n) reaction: new opportunities for medical alpha emitter ^{149}Tb production. Sci. Rep. **10**, 508 (2020). https://doi.org/10.1038/s41598-020-57436-6
8. B. Webster, P. Ivanov, B. Russell et al., Chemical purification of terbium-155 from pseudo-isobaric impurities in a mass separated source produced at CERN. Sci. Rep. **9**, 10884 (2019). https://doi.org/10.1038/s41598-019-47463-3
9. C. Vermeulen, G. Steyn, F. Szelecsényi et al., Cross sections of proton-induced reactions on Gd with special emphasis on the production possibilities of ^{152}Tb and ^{155}Tb. Nucl. Instrum. Methods Phys. Res. Sect. B **275**, 24–32 (2012). https://doi.org/10.1016/j.nimb.2011.12.064
10. G. Steyn, C. Vermeulen, F. Szelecsényi et al., Cross sections of proton-induced reactions on ^{152}Gd, ^{155}Gd and ^{159}Tb with emphasis on the production of selected Tb radionuclides. Nucl.

Instrum. Methods Phys. Res. Sect. B **319**, 128–140 (2014). https://doi.org/10.1016/j.nimb.2013.11.013
11. R.T. Güray, N. Özkan, C. Yalçın et al., Measurements of ^{152}Gd(p,γ)^{153}Tb and ^{152}Gd(p, n)^{152}Tb reaction cross sections for the astrophysical γ process. Phys. Rev. C **91**, 055809 (2015). https://doi.org/10.1103/PhysRevC.91.055809
12. F. Tárkányi, S. Takács, F. Ditrói et al., Activation cross-sections of deuteron induced reactions on ^{nat}Gd up to 50 MeV. Appl. Radiat. Isot. **83**, 25–35 (2014). https://doi.org/10.1016/j.apradiso.2013.10.010
13. Gy. Gyürky, Z. Elekes, J. Farkas et al., Alpha-induced reaction cross section measurements on ^{151}Eu for the astrophysical γ-process. J. Phys. G Nucl. Part. **37**, 115201 (2010). https://doi.org/10.1088/0954-3899/37/11/115201
14. A. Moiseeva, R. Aliev, V. Unezhev et al., Alpha particle induced reactions on ^{151}Eu: Possibility of production of ^{152}Tb radioisotope for PET imaging. Nucl. Instrum. Methods Phys. Res. Sect. B **497**, 59–64 (2021). https://doi.org/10.1016/j.nimb.2021.04.007
15. C. Müller, C. Vermeulen, K. Johnston et al., Preclinical in vivo application of ^{152}Tb-DOTANOC: a radiolanthanide for PET imaging. EJNMMI Res. **6**, 35 (2016). https://doi.org/10.1186/s13550-016-0189-4
16. M. Eroğlu, C. Yalçın, R.T. Güray, Investigation of the ^{121}Sb(α,γ)^{125}I reaction cross-section calculations at astrophysical energies. Nucl. Sci. Tech. **34**, 168 (2023). https://doi.org/10.1007/s41365-023-01301-4
17. C. Yalçın, The cross section calculation of ^{112}Sn(α,γ)^{116}Te reaction with different nuclear models at the astrophysical energy range. Nucl. Sci. Tech. **28**, 113 (2017). https://doi.org/10.1007/s41365-017-0267-y
18. R. Baldık, A. Yılmaz, A study on the excitation functions of ^{60,62}Ni(α, n), ^{60,61}Ni(α,2n), ^{58,64}Ni(α, p), ^{nat}Ni(α, x) reactions. Nucl. Sci. Tech. **29**, 156 (2018). https://doi.org/10.1007/s41365-018-0500-3
19. J.H. Luo, J.C. Liang, L. Jiang et al., Measurement of ^{134}Xe(n,2n)^{133m,g}Xe reaction cross sections in 14-MeV region with detailed uncertainty quantification. Nucl. Sci. Tech. **34**, 4 (2023). https://doi.org/10.1007/s41365-022-01158-z
20. R. Kruse, C. Borgelt, F. Klawonn et al., *Computational Intelligence* (Springer, London, 2013), p.15
21. Z. Korkulu, N. Özkan, G.G. Kiss et al., Investigation of α -induced reactions on Sb isotopes relevant to the astrophysical γ process. Phys. Rev. C **97**, 045803 (2018). https://doi.org/10.1103/PhysRevC.97.045803
22. N. Özkan, R.T. Güray, C. Yalçın et al., Proton capture reaction cross section measurements on ^{162}Er as a probe of statistical model calculations. Phys. Rev. C **96**, 045805 (2017). https://doi.org/10.1103/PhysRevC.96.045805
23. C. Yalçın, Gy. Gyürky, T. Rauscher et al., Test of statistical model cross section calculations for α-induced reactions on ^{107}Ag at energies of astrophysical interest. Phys. Rev. C **91**, 034610 (2015). https://doi.org/10.1103/PhysRevC.91.034610
24. R.T. Güray, N. Özkan, C. Yalçın et al., Measurements of proton-induced reaction cross sections on ^{120}Te for the astrophysical p process. Phys. Rev. C **80**, 035804 (2009). https://doi.org/10.1103/PhysRevC.80.035804
25. C. Yalçın, R.T. Güray, N. Özkan et al., Odd p isotope ^{113}In: measurement of α-induced reactions. Phys. Rev. C **79**, 065801 (2009). https://doi.org/10.1103/PhysRevC.79.065801
26. F. Ditroi, S. Takacs, F. Tarkanyi et al., Thin layer activation of large areas for wear study. Wear **261**, 1397–1400 (2006). https://doi.org/10.1016/j.wear.2006.03.0
27. A.J. Koning, S. Hilaire, S. Goriely, TALYS: modeling of nuclear reactions. Eur. Phys. J. A **59**, 131 (2023). https://doi.org/10.1140/epja/s10050-023-01034-3
28. S. Watanabe, High energy scattering of deuterons by complex nuclei. Nucl. Phys. **8**, 484 (1958). https://doi.org/10.1016/0029-5582(58)90180-9
29. L. McFadden, G.R. Satchler, Optical-model analysis of the scattering of 24.7 MeV alpha particles. Nucl. Phys. **84**, 177 (1966). https://doi.org/10.1016/0029-5582(66)90441-X
30. P. Demetriou, C. Grama, S. Goriely, Improved global α-optical model potentials at low energies. Nucl. Phys. A **707**, 253 (2002). https://doi.org/10.1016/S0375-9474(02)00756-X
31. V. Avrigeanu, M. Avrigeanu, C. Manailescu, Further explorations of the α-particle optical model potential at low energies for the mass range $A\approx$45–209. Phys. Rev. C **90**, 044612 (2014). https://doi.org/10.1103/PhysRevC.90.044612
32. M. Nolte, H. Machner, J. Bojowald, Global optical potential for α particles with energies above 80 MeV. Phys. Rev. C **36**, 1312 (1987). https://doi.org/10.1103/PhysRevC.36.1312
33. V. Avrigeanu, P.E. Hodgson, M. Avrigeanu, Global optical potentials for emitted alpha particles. Phys. Rev. C **49**, 2136 (1994). https://doi.org/10.1103/PhysRevC.49.2136
34. A. Gilbert, A.G.W. Cameron, A composite nuclear-level density formula with shell corrections. Can. J. Phys. **43**, 1446 (1965). https://doi.org/10.1139/p65-139
35. W. Dilg, W. Schantl, H. Vonach et al., Level density parameters for the back-shifted Fermi gas model in the mass range $40 < A < 250$. Nucl. Phys. A **217**, 269 (1973). https://doi.org/10.1016/0375-9474(73)90196-6
36. P. Demetriou, S. Goriely, Microscopic nuclear level densities for practical applications. Nucl. Phys. A **695**, 95 (2001). https://doi.org/10.1016/S0375-9474(01)01095-8
37. A.V. Ignatyuk, K.K. Istekov, G.N. Smirenkin, The role of collective effects in the systematics of nuclear level densities. Sov. J. Nucl. Phys. **29**, 875–883 (1979)
38. A.V. Ignatyuk, J.L. Weil, S. Raman et al., Density of discrete levels in ^{116}Sn. Phys. Rev. C **47**, 1504 (1993). https://doi.org/10.1103/PhysRevC.47.1504
39. S. Goriely, S. Hilaire, A.J. Koning, Improved microscopic nuclear level densities within the Hartree-Fock-Bogoliubov plus combinatorial method. Phys. Rev. C **78**, 064307 (2008). https://doi.org/10.1103/PhysRevC.78.064307
40. S. Hilaire, S. Goriely, Global microscopic nuclear level densities within the HFB plus combinatorial method for practical applications. Nucl. Phys. A **779**, 63 (2006). https://doi.org/10.1016/j.nuclphysa.2006.08.014
41. S. Hilaire, M. Girod, S. Goriely et al., Temperature-dependent combinatorial level densities with the D1M Gogny force. Phys. Rev. C **86**, 064317 (2012). https://doi.org/10.1103/PhysRevC.86.064317
42. J. Kopecky, M. Uhl, R.E. Chrien, Radiative strength in the compound nucleus ^{157}Gd. Phys. Rev. C **47**, 312 (1993). https://doi.org/10.1103/PhysRevC.47.312
43. J. Kopecky, M. Uhl, Test of gamma-ray strength functions in nuclear reaction model calculations. Phys. Rev. C **41**, 1941 (1990). https://doi.org/10.1103/PhysRevC.41.1941
44. D.M. Brink, Individual particle and collective aspects of the nuclear photoeffect. Nucl. Phys. **4**, 215 (1957). https://doi.org/10.1016/0029-5582(87)90021-6
45. P. Axel, Electric dipole ground-state transition width strength function and 7-MeV photon interactions. Phys. Rev. **126**, 671 (1962). https://doi.org/10.1103/PhysRev.126.671
46. S. Goriely, E. Khan, Large-scale QRPA calculation of E1-strength and its impact on the neutron capture cross section.

Nucl. Phys. A **706**, 217 (2002). https://doi.org/10.1016/S0375-9474(02)00860-6
47. S. Goriely, E. Khan, M. Samyn, Microscopic HFB + QRPA predictions of dipole strength for astrophysics applications. Nucl. Phys. A **739**, 331 (2004). https://doi.org/10.1016/j.nuclphysa.2004.04.105
48. S. Goriely, Radiative neutron captures by neutron-rich nuclei and the r-process nucleosynthesis. Phys. Lett. B **436**, 10 (1998). https://doi.org/10.1016/S0370-2693(98)00907-1
49. D.P. Arteaga, P. Ring, Relativistic random-phase approximation in axial symmetry. Phys. Rev. C **77**, 034317 (2008). https://doi.org/10.1103/PhysRevC.77.034317
50. M. Martini, S. Hilaire, S. Goriely et al., Improved nuclear inputs for nuclear model codes based on the Gogny interaction. Nucl. Data Sheets **118**, 273 (2014). https://doi.org/10.1016/j.nds.2014.04.056
51. S. Hilaire, M. Girod, S. Goriely et al., Temperature-dependent combinatorial level densities with the D1M Gogny force. Phys. Rev. C **86**, 064317 (2012). https://doi.org/10.1103/PhysRevC.86.064317
52. V. Plujko, O. Gorbachenko, K. Solodovnyk, Description of nuclear photoexcitation by Lorentzian expressions for electric dipole photon strength function. Eur. Phys. J. A **55**, 1–12 (2019). https://doi.org/10.1140/epja/i2019-12899-6
53. National Nuclear Data Center (NNDC). http://www.nndc.bnl.gov/nudat3. Accessed 11 May 2024
54. N. Otuka, S. Takács, Definitions of radioisotope thick target yields. Radiochim. Acta **103**, 1–6 (2014). https://doi.org/10.1515/ract-2013-2234
55. W.R. Leo, *Techniques for Nuclear and Particle Physics Experiments* (Springer, Berlin, 1994)
56. C. Yalçın, Thickness measurement using alpha spectroscopy and SRIM. J. Phys. **590**, 012050 (2015). https://doi.org/10.1088/1742-6596/590/1/012050
57. P. Mohr, Gy. Gyürky, Zs. Fülöp, Statistical model analysis of γ -induced reaction cross sections of ^{64}Zn at low energies. Phys. Rev. C **95**, 015807 (2017). https://doi.org/10.1103/PhysRevC.95.015807